2017-05

Nothing more than a pair of curvatures: A common mechanism for the detection of both radial and non-radial frequency patterns

KANG, JUNGHEE

10.1016/j.visres.2017.03.005
Vision Research
Elsevier BV

Vision Research 134 (2017) 18–25

Contents lists available at ScienceDirect

Vision Research

journal homepage: www.elsevier.com/locate/visres

Nothing more than a pair of curvatures: A common mechanism for the detection of both radial and non-radial frequency patterns

Gunnar Schmidtmann *, Frederick A.A. Kingdom

McGill Vision Research, Department of Ophthalmology, McGill University, Canada

ARTICLE INFO

Article history:
Received 20 June 2016
Received in revised form 19 March 2017
Accepted 20 March 2017

Keywords:
Radial frequency patterns
Curvature
Curvature detection

ABSTRACT

Radial frequency (RF) patterns, which are sinusoidal modulations of a radius in polar coordinates, are commonly used to study shape perception. Previous studies have argued that the detection of RF patterns is either achieved globally by a specialized global shape mechanism, or locally using as cue the maximum tangent orientation difference between the RF pattern and the circle. Here we challenge both ideas and suggest instead a model that accounts not only for the detection of RF patterns but also for line frequency patterns (LF), i.e. contours sinusoidally modulated around a straight line. The model has two features. The first is that the detection of both RF and LF patterns is based on curvature differences along the contour. The second is that this curvature metric is subject to what we term the *Curve Frequency Sensitivity Function,* or CFSF, which is characterized by a flat followed by declining response to curvature as a function of modulation frequency, analogous to the modulation transfer function of the eye. The evidence that curvature forms the basis for detection is that at very low modulation frequencies (1–3 cycles for the RF pattern) there is a dramatic difference in thresholds between the RF and LF patterns, a difference however that disappears at medium and high modulation frequencies. The CFSF feature on the other hand explains why thresholds, rather than continuously declining with modulation frequency, asymptote at medium and high modulation frequencies. In summary, our analysis suggests that the detection of shape modulations is processed by a common curvature-sensitive mechanism that is subject to a shape-frequency-dependent transfer function. This mechanism is independent of whether the modulation is applied to a circle or a straight line.

1. Introduction

Radial frequency (RF) patterns are closed shapes, which are defined by a sinusoidal modulation of a radius in polar coordinates. Since their introduction (Wilkinson, Wilson, & Habak, 1998), RF patterns have become a popular class of stimuli in vision science, commonly used to study various aspects of shape perception. Theoretically, RF pattern detection (discrimination against a circle) could be realized either by local filters matched to the parts of the pattern, or by a global mechanism that integrates local parts operating on the scale of the entire pattern. Wilkinson et al. (1998) measured RF detection thresholds (circle vs. RF) as a function of frequency (RF1–RF24), and argued that the pattern of thresholds could not be explained by local analyses of either orientation or curvature. The maximum orientation difference between an RF and a circle for a given amplitude is proportional to radial frequency (see below), so if orientation was the cue, thresholds would be expected to decline linearly (on a log-log plot) with modulation frequency. However, Wilkinson et al. showed that while thresholds did decline at low RFs (up to RF3) they were constant for higher RFs up to the frequency of 24 that was tested. A similar argument led to a rejection of maximum curvature as the cue, which also predicts a continuous decline in thresholds, this time in proportion to the square of radial frequency. Instead, Wilkinson et al. (1998) proposed that local information was pooled into a global representation of shape. The idea was subsequently developed by Poirier and Wilson (2006), Dickinson, Bell, and Badcock (2013) and Kempgens, Loffler, and Orbach (2013), who proposed global models for RF shapes that integrated local maximum curvature information. Support for a global shape model of RF processing also came from a number of psychophysical studies of RF detection (Bell & Badcock, 2008; Bell, Badcock, Wilson, & Wilkinson, 2007; Bell, Wilkinson, Wilson, Loffler, & Badcock, 2009; Dickinson, McGinty, Webster, & Badcock, 2012; Dickinson et al., 2013; Hess, Achtman, & Wang, 2001; Hess, Wang, & Dakin, 1999; Jeffrey, Wang, & Birch, 2002; Loffler, Wilson, & Wilkinson,

* Corresponding author.
E-mail addresses: gunnar.schmidtmann@mail.mcgill.ca (G. Schmidtmann), fred.kingdom@mcgill.ca (F.A.A. Kingdom).

http://dx.doi.org/10.1016/j.visres.2017.03.005
0042-6989/

2003; Schmidtmann, Kennedy, Orbach, & Loffler, 2012; Tan, Dickinson, & Badcock, 2013), as well as psychophysical studies investigating suprathreshold RF shape aftereffects (Bell, Gheorghiu, Hess, & Kingdom, 2011; Bell, Hancock, Kingdom, & Peirce, 2010).

Some recent studies, however, have challenged these conclusions. Mullen, Beaudot, and Ivanov (2011) measured detection thresholds for RF patterns with modulation frequencies between 2 and 20, as well as sinusoidally modulated lines, referred to here as line frequency or LF patterns, with modulation frequencies ranging from 1 to 20. Over the range of common frequencies (2–20), thresholds were similar for the two types of pattern. In keeping with similar proposals in previous studies dealing exclusively with LF patterns (Prins, Kingdom, & Hayes, 2007; Tyler, 1973), Mullen et al. (2011) suggested that the critical features underlying detection for both RF and LF patterns were the differences between the tangent orientations at consecutive inflection points along the waveforms. These inflection-point tangent-orientation differences are the maximum orientation differences for an LF pattern and, when centred on the peaks, the maximum orientation differences for an RF pattern. Based on these tangent orientation differences, Mullen et al. proposed different model variants for LF and RF patterns, and showed that with a suitable adjustment of each model's free parameters, the two models could be fit to the data for frequencies between 2 and 6 (a critical discussion of Mullen et al.'s model can be found in Dickinson et al., 2012). Note incidentally that Wilkinson et al. (1998) also observed similar thresholds between LF and RF, but rejected a common mechanism on the grounds that RF and LF thresholds showed a different dependence on contrast.

Another study that has questioned previous views on RF detection is that of Baldwin, Schmidtmann, Kingdom, and Hess (2016). The context for this study are the aforementioned threshold studies investigating RF summation, in which RF detection thresholds were measured as a function of the number of modulated RF cycles (Bell et al., 2007, 2009; Bell & Badcock, 2008; Dickinson et al., 2012; Hess et al., 1999; Loffler et al., 2003; Schmidtmann et al., 2012; Tan et al., 2013). The amount of summation in these experiments typically exceeded the prediction expected from a system where each RF cycle was detected independently, i.e. by probability summation, assuming a High Threshold Theory (HTT) model of detection. This was taken as evidence for a global pooling mechanism for RF patterns. However, Baldwin et al. (2016) showed that the detection of RF patterns followed the predictions of Signal Detection Theory (SDT) rather than HTT, in keeping with the belief that SDT is categorically the better model of detection (Green & Swets, 1988; Kingdom, Baldwin, & Schmidtmann, 2015; Laming, 2013; Nachmias, 1981). Moreover, when modelled under SDT, Baldwin et al. (2016) showed that probability summation could *not* be rejected as a model of RF summation. This result therefore also raises the possibility that alternative, non-global mechanisms might underpin RF detection. The significance here is that if non-global mechanisms underpin RF pattern detection, a common mechanism for LF and RF pattern detection becomes a real possibility, because LF patterns are themselves inherently more likely to be detected by a non-global rather than global mechanism.

In this communication we are interested in whether the *same* model can account for *both* RF and LF data across the *full range* of frequencies (1–20), *without change of parameters*. As it stands, a model based on the orientation differences at consecutive inflections within the waveform does not account for the profound differences in thresholds between RF and LF patterns at very low frequencies that we and others find, nor does it predict the asymptotic thresholds at middle and high frequencies. We suggest instead a new model based on the detection of curvature differences to account for the pattern of thresholds observed in both RF and LF patterns. We demonstrate that this model not only predicts the initial differences between RF and LF patterns for low frequencies, but also the asymptotic thresholds in these patterns for high modulation frequencies. We have tested our model against existing data as well as new data obtained using both RF and LF patterns at a wide range of frequencies.

2. Methods

2.1. Subjects

Four observers participated in this study. Three were naïve as to the purpose of the study. Subjects had normal or corrected-to-normal visual acuity. Informed consent was obtained from each observer. All experiments were approved by the McGill University Ethics committee and were conducted in accordance with the original Declaration of Helsinki.

2.2. Apparatus

The stimuli were generated using MATLAB (MATLAB R 2015b, MathWorks) and presented on a gamma-corrected Iiyama Vision Master Pro 513 CRT monitor running with a resolution of 1600×1200 pixels and a frame rate of 60 Hz (mean luminance 40 cd/m^2), under the control of an Apple Mac Pro (3.33 GHz). Observers viewed the stimuli at a distance of 200 cm. At this viewing distance one pixel subtended 0.0072° of visual angle. Experiments were performed in a dimly illuminated room. Routines from the Psychophysics Toolbox were employed to present the stimuli (Brainard, 1997).

2.3. Stimuli

The aim of this study was to compare the detection of RF and LF patterns. Both stimulus types were white and presented on a mid grey background. The RF patterns are defined by sinusoidal modulations of a radius in polar coordinates (Wilkinson et al., 1998).

$$r(\theta) = r_{mean}[1 + Asin(\omega\theta + \varphi)] \quad (1)$$

where r (radius) and θ refer to the polar coordinates of the contour and r_{mean} is the radius of the modulated circle, which was set to 0.715 deg. The variable A defines the modulation amplitude, ω the radial frequency and φ the phase (orientation), where the latter was randomly varied on a trial to trial basis. In order to compare thresholds for RF and LF patterns we express the RF modulation depth not as a proportion of the radius r_{mean}, as with amplitude A in Eq. (1), but in common units of degrees of visual angle. By expanding Eq. (1), one can see that this is given by the product of A and r_{mean}. Twelve frequencies ω were used: 1, 2, 3, 4, 6, 8, 10, 12, 14, 16 18 and 20. The cross-sectional luminance profile was defined by a Gaussian with a standard deviation of 0.05 deg. The phase φ was pseudo-randomly varied on a trial-to-trial basis.

The LF patterns consisted of two horizontal lines, which were modulated in a sinusoidal manner with the same frequencies as the RF patterns:

$$l(\theta) = Asin(\omega\theta + \varphi) \quad (2)$$

where A is expressed in degrees of visual angle. The modulation frequency was the same in both lines. For example, Fig. 1B shows a frequency of six, where the upper and lower line each contains three cycles. The combined length of both lines was set to the circumference of the corresponding RF pattern (C_{RF}), which was calculated according to:

$$C_{RF} = \int_0^{2\pi} \sqrt{r'(\theta)^2 + r(\theta)}d\theta \quad (3)$$

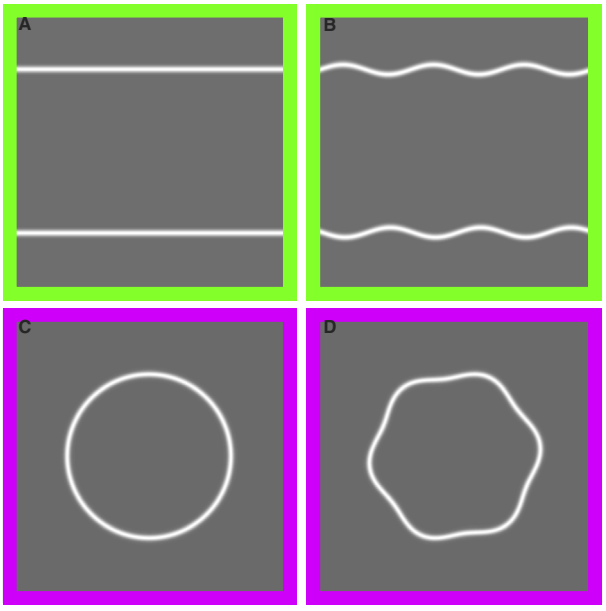

Fig. 1. Schematic of stimuli used in this study. The top row shows the LF and the bottom row the RF stimuli used in this study. (A) and (C) illustrate the reference patterns, i.e. two straight lines in the case of the LF stimuli and a circle in the case of the RF patterns. For illustration purposes, both test patterns are shown with a supra-threshold modulation amplitude and a frequency of six.

The distance between the two lines was set to the diameter of the RF patterns (1.43°). The phases of the sinusoidal modulations for each line were randomly determined from trial to trial and were different between the top and bottom line.

2.4. Procedure

The method of constant stimuli was employed in conjunction with a temporal two-alternative forced choice paradigm. Observers were presented with two patterns, a test and a reference (see Fig. 1). The monitor's background was initially set to a mean luminance (grey). Stimulus presentation time was 180 ms with a pre-and inter-stimulus interval of 400 ms. The task for the observer was to choose the test stimulus by pressing one of two keys on a numeric keypad. The order of test and reference stimuli was random. The spatial location of the stimuli was randomly varied from trial to trial with a horizontal and vertical positional jitter of ±0.36° with respect to the centre of the screen. Seven different linearly spaced modulation amplitudes *A* were tested in each experimental block. Each modulation amplitude was tested 30 times, leading to 210 measurements. Percent correct responses were calculated and the resulting data were fit with a Quick psychometric function (Quick, 1974) using a customized maximum-likelihood procedure based on binomial proportions, using MatLab's *fminsearch* function. Detection thresholds were defined as the modulation amplitude yielding 75% correct responses. The LF and RF patterns were tested in separate blocks. Observers usually completed two experimental blocks for each experimental condition and their results were averaged.

3. Results

3.1. Radial frequency vs. line frequency stimuli

Fig. 2A shows detection thresholds expressed as the modulation amplitude in degree visual angle as a function of modulation frequency for RF (magenta) and LF (green) patterns. The graph shows individual data presented by the empty data points (GS: ○, MO: ×, BJ: △, SB: ▷), as well as results averaged across subjects illustrated by the solid data points and lines. The shaded regions represent 95% confidence intervals.

Detection thresholds for RF patterns decrease with increasing frequency and asymptote at a frequency of about 6. For the lowest frequencies ($\omega = 1$), detection thresholds for RF patterns are on average about 17 times higher than thresholds for LF patterns. Detection thresholds for the LF patterns decreased with increasing modulation frequency, but the decline is less pronounced at low frequencies compared to RF patterns. Results were statistically analyzed using a two-factor (stimulus type; frequency) repeated measure ANOVA. This analysis revealed a statistically significant interaction between stimulus type (RF, LF) and frequency ($F_{11,33} = 377$, $p < 0.001$). Subsequent post hoc tests (Bonferroni

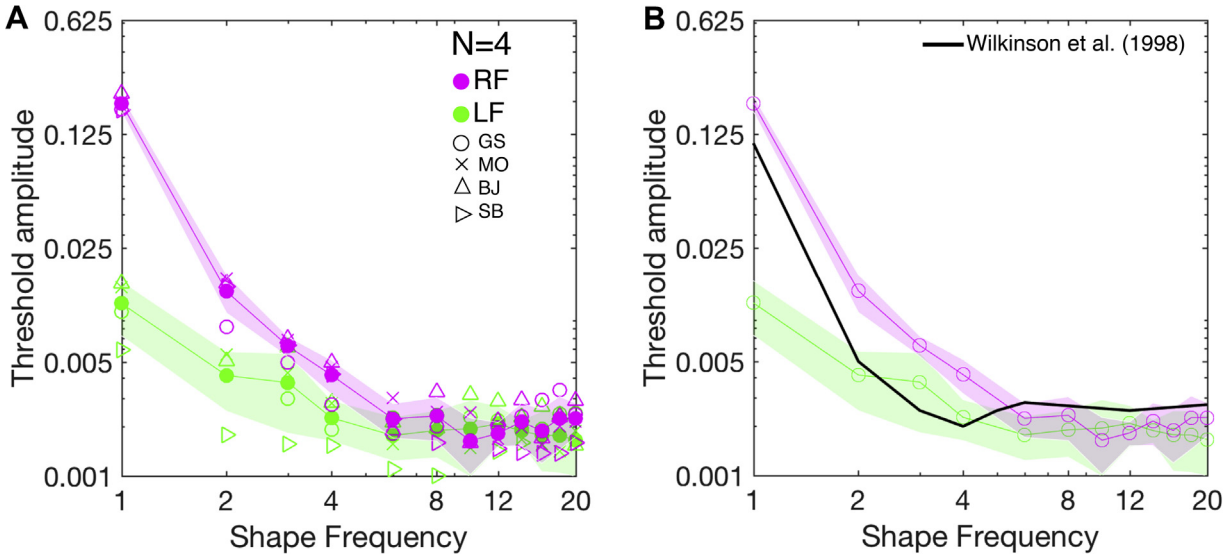

Fig. 2. Detection thresholds for RF (magenta) and LF (green) patterns as a function of modulation frequency. Thresholds are expressed as modulation amplitude in visual angle (deg). The shaded regions represent 95% confidence intervals. (A) shows individual threshold for each observer (N = 4; empty data points) as well as the data averaged across subjects (solid data points, solid lines). The black solid line in (B) shows results by Wilkinson et al. (1998) for RF patterns. (For interpretation of the references to colour in this figure legend, the reader is referred to the web version of this article.)

corrected) showed that thresholds for $\omega = 1$ and $\omega = 2$ were significantly different between RF and LF patterns (RF1: $p < 0.001$; RF2: $p < 0.01$), but thresholds did not significantly differ between RF and LF patterns for all other tested frequencies. In a control experiment, detection thresholds for LF and RF patterns with modulation frequencies of $\omega = 20$ and $\omega = 30$ were measured for two additional observers. The data were statistically analyzed with a repeated measure ANOVA with shape type (RF and LF) and modulation frequency ($\omega = 20$ and 30) as factors. Results show that thresholds are not statistically significant between shape types ($F_{1,3} = 0.704$, $p = 0.463$) and frequency ($F_{1,3} = 2.807$, $p = 0.192$).

In summary, detection thresholds for RF and LF patterns are very different for frequencies between 1 and 2, across which they decline (and rapidly for the RF pattern), coincide for frequencies beyond 3–4 and asymptote for higher frequencies. The pattern of results for RF patterns is consistent with previous results by Wilkinson et al. (1998). Their results for one subject (FW in their Fig. 3) were converted into visual angle and are illustrated by the solid black line in Fig. 2B. Note, that Wilkinson et al. (1998) used RF patterns with a slightly smaller radius of 0.5°. The results are also similar to the results from Mullen et al. (2011), who showed that thresholds for radial frequencies were similar to those of line stimuli. The thresholds were higher in Mullen et al.'s study, most likely due to their stimulus design (see Discussion for details).

3.2. Model

The aim of the current study is to provide a single model that can explain the observed pattern of results for both RF and LF patterns across the full range of frequencies ($\omega = 1$–20). The model we propose is based on curvature. For an LF pattern, curvature (κ_{LF}) is based on the first and second derivatives of Eq. (2), which are respectively:

$$l'(\theta) = A\omega \cos(\omega\theta) \tag{4}$$

and

$$l''(\theta) = -A\omega^2 \sin(\omega\theta) \tag{5}$$

The curvature κ_{LF} of an LF pattern is then given by:

$$\kappa_{LF}(\theta) = \frac{l''(\theta)}{\left(1 + \left(l'(\theta)^2\right)\right)^{3/2}} \tag{6}$$

The equation for the RF pattern is:

$$r(\theta) = r_{mean}[1 + A\sin(\omega\theta + \varphi)] \tag{7}$$

By expanding Eq. (7) one can see that the modulation depth in units of visual angle is given by $r_{mean}\,A$, with A defined as a fraction of r_{mean}. In order to express A in the same units for both RF and LF patterns we therefore set r_{mean} to unity. The first and second derivatives for an RF pattern are then given by:

$$r'(\theta) = A\omega\cos(\omega\theta + \varphi) \tag{8}$$

$$r''(\theta) = -A\omega^2\sin(\omega\theta + \varphi) \tag{9}$$

and

$$\kappa_{RF}(\theta) = \frac{r(\theta)^2 + 2r'(\theta)^2 - r(\theta)r''(\theta)}{\left(r(\theta)^2 + r'(\theta)^2\right)^{3/2}} \tag{10}$$

Fig. 3 shows the dependence of the pattern of curvature difference between the waveform and its underlying baseline (circle for RF,

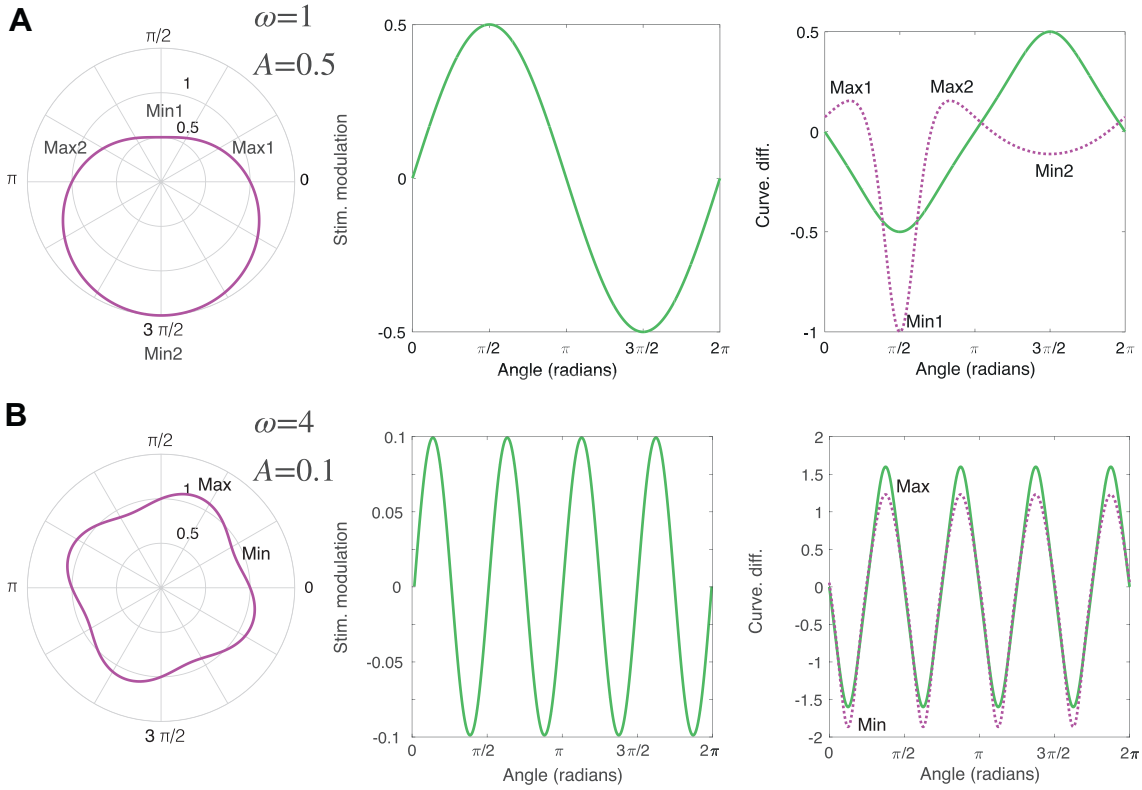

Fig. 3. Top (A), left: RF pattern; middle: LF pattern; right, curvature differences between waveform and baseline (RF magenta, LF green); all for $\omega = 1$. Bottom (B), corresponding figures for $\omega = 4$. For illustration purposes, the modulation amplitudes A for the $\omega = 1$ and $\omega = 4$ patterns were set to 0.5 and 0.1 respectively, which is well above threshold. Angle is given in radians around the full circle of an RF. Min1, Min2 and Max1, Max2 (for RF1) and Max and Min (RF4) refer to local peaks and troughs in curvature difference. The metric proposed to underlie detection is the largest Max-Min difference. (For interpretation of the references to colour in this figure legend, the reader is referred to the web version of this article.)

straight line for LF) on the modulation frequency of the RF and LF pattern. Fig. 3A (leftmost) shows an RF1 pattern with a modulation amplitude of $A = 0.5$. At such a high amplitude it becomes clear that the RF1 is a special case with respect to its curvature difference along the waveform, which is presented in the rightmost graph (magenta). Min and Max refer to the points of local minimum and local maximum curvature. These points are also illustrated in the rightmost graph, which shows the curvature difference between the waveform and its baseline. The waveform of an LF1 pattern (green) shown in the middle panel, on the other hand, has one point of maximum and minimum curvature. This difference in the *pattern* of minima/maxima between RF and LF patterns does not exist for modulation frequencies higher than 1, as can be seen in Fig. 3B. The modulation *depths* of the curvature differences differ substantially between RF1 and LF1, with much smaller values for the former. For the F4 case the curvature difference modulation depth is only slightly less for RF compared to LF.

Fig. 4A shows how a metric defined by the difference between maximum and minimum curvature (referred to as: Max–Min curvature) for both RF (magenta) and non-RF stimuli (green) changes as a function of modulation frequency, this time for a fixed modulation amplitude of $A = 0.01$ and an r_{mean} of unity. It is evident that this curvature-based metric predicts the pronounced difference between RF and LF patterns for the low frequency range ($\omega = 1$–2) as well as the subsequent convergence of thresholds at higher frequencies, consistent with the observed pattern of results. However, the metric does not explain the asymptotic thresholds at higher modulation frequencies. To account for this asymptotic behavior, we introduce the *Curve Frequency Sensitivity Function,* or CSFF, which is characterized by a flat followed by declining response to curvature as a function of modulation frequency. The decline in response to curvature at high modulation frequencies embodies the idea of a perceptual limitation for high curve frequencies, and is illustrated in Fig. 4B.

The *CFSF* is defined as:

$$CFSF = \left(1 + \left(\frac{\omega}{a}\right)^2\right)^{-b} \tag{11}$$

an equation based on a formula for the mean radial modulation transfer function provided by Watson (2013), where ω refers to the modulation frequency and a and b are constants. To incorporate the *CFSF* into the model we divided the curvature amplitudes by the *CFSF*. The overall model has three free parameters, the constants a, b in Eq. (11) and the Max-Min curvature amplitude threshold. In order to determine the model thresholds T_M the following term was minimized using the *PAL_minimize* function in the Palamedes Toolbox (Prins & Kingdom, 2009):

$$T_M = \sum \left(\frac{M_{LF} - D_{LF}}{D_{LF}}\right)^2 + \sum \left(\frac{M_{RF} - D_{RF}}{D_{RF}}\right)^2 \tag{12}$$

where M refers to the model and D to the data. It is very important to emphasize that a single model is fitted simultaneously to both the LF and RF data. The three fitted free parameters of the model are the Max-Min curvature amplitude threshold = 0.0287, and the two CFSF (Eq. (11)) parameters a = 2.82 and b = 0.9605. The model fits are shown in Fig. 5. The model captures the initial large threshold difference between RF and LF patterns for low modulation frequencies, as well as the subsequent deceleration with increasing

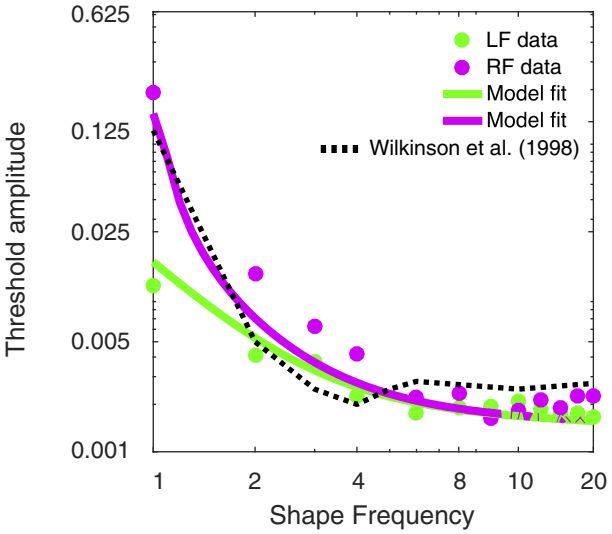

Fig. 5. The graph shows the single model fits (solid lines) to both RF and LF data (filled dots replotted from Fig. 2B). The black dotted line is the RF data from Wilkinson et al. (1998).

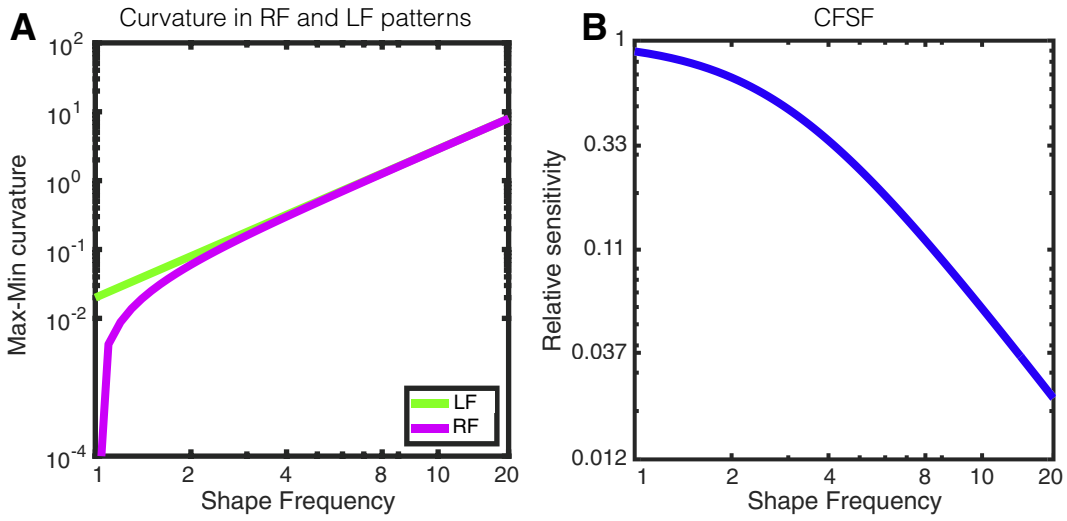

Fig. 4. (A) Maximum minus minimum curvature for LF (green) and RF (magenta) patterns as a function of modulation frequency for a fixed modulation amplitude of $A = 0.01$, and with r_{mean} set to unity for the RF patterns. (B) Fitted *CFSF* (Curvature Frequency Sensitivity Function). The plot shows relative sensitivity as a function of modulation frequency as fitted to both the RF and LF data. (For interpretation of the references to colour in this figure legend, the reader is referred to the web version of this article.)

frequency. The goodness of fit between the model and the data was evaluated by calculating the coefficient of determination R^2. R^2 for the single fit to both LF and RF data is 0.996. For the same single fit (i.e. to both LF and RF data), R^2 for the LF data alone is 0.989 and for the RF data alone 0.999. Note that R^2 compares relative sizes, not absolute sizes. Despite the very high values of R^2, there is a modest, systematic mismatch between the model and the data, namely, the model underestimates the experimental RF thresholds, especially in the 2–4 range of shape frequency.

4. Discussion

The aim of the current study is to demonstrate that a model based on the detection of curvature differences can explain the observed pattern of thresholds for both RF and LF patterns across the full range of frequencies. We showed that a combination of two model features, first curvature detection, second a function that describes how sensitivity to curvature falls with curvature frequency, gave a good account of performance with both types of pattern. Our model was fit simultaneously to both RF and LF data, i.e. with no parameter differences.

The curvature based model proposed here has the advantage that it explains both RF and LF detection thresholds across the full range of modulation frequency. Previous studies have either suggested different model variants for RF and LF patterns modelled across a narrow range of modulation frequencies (Mullen et al., 2011), or, in the case of RF patterns, two separate mechanisms, one for low and one for high radial frequencies (Jeffrey et al., 2002; Loffler et al., 2003; Schmidtmann et al., 2012). The latter dual-mechanism RF model gained support from the observation that global pooling, not probability summation, was evident for low radial frequencies (RF3, RF5 and partially for RF10, Loffler et al., 2003), but not for higher radial frequencies (e.g. RF24). However, as we noted in the Introduction, a note of caution comes from Baldwin et al. (2016) who showed that, when modelled under Signal Detection Theory, probability summation can *not* be rejected as a model of RF summation, even for low modulation frequencies ($\omega = 4$).

That curvature is the feature underpinning RF detection finds expression in a number of early models of single curve detection/discrimination (Watt & Andrews, 1982; Wilson, 1985; Wilson & Richards, 1989) as well as later models explicitly dealing with RF shapes (Dickinson et al., 2013; Kempgens et al., 2013; Poirier & Wilson, 2006). In the latter models the location of points of maximum curvature around the RF are encoded and form the input to the final stage that encodes the RF's global shape. Our model calculates the difference between maximum and minimum curvature. We speculate that this might occur at intermediate levels of visual processing involving mechanisms that calculate curvature over a 1/2 cycle centered on the maxima/minima, as suggested by psychophysical shape adaptation studies using suprathreshold-shape stimuli (Gheorghiu & Kingdom, 2007, 2009). This is in keeping with functional magnetic resonance imaging (fMRI) studies showing that radial and concentric gratings (Wilkinson et al., 2000), as well as Gabor flow-fields containing contours (Dumoulin & Hess, 2007), evoke stronger responses at intermediate level visual areas V3 and hV4 compared to areas V1 or V2. More recently, Salmela, Henriksson, and Vanni (2016) investigated RF shape representation using a multi-voxel pattern analysis and suggested that the RF specific representations are in areas V2d, V3d, V3AB, and IPS0, not hV4 or LO. The above differences in fMRI studies are most likely due to the analysis approach. The advantage of multi-voxel pattern analysis is that the multidimensional pattern of activity across voxels contains more information compared to averaged one-dimensional measures (Kriegeskorte & Kievit, 2013; Kriegeskorte, Mur, & Bandettini, 2008). In addition, the searchlight-based procedure employed by Samela et al. makes no assumptions with respect to where the activation pattern should occur (Kriegeskorte, Goebel, & Bandettini, 2006).

It is important to bear in mind that our model is agnostic to whether the curvature information from each cycle of the pattern, whether LF or RF, is pooled additively into a global detection mechanism or combined by probability summation. In fact, our model involves no pooling of curvature-difference information across the stimulus. An anonymous reviewer correctly pointed out that our model could incorporate summation of curvature-differences across the various cycles of the waveforms, and indeed this would have been more realistic. However, if we were to incorporate either additive or probability summation for the two types of pattern, the effect would only be to change the values of the parameters of the CFSF when fit to the data. The CFSF model proposed here embodies the effects of summation (whether additive or probability) in the same way that a model of the high-frequency decline in grating contrast sensitivity for gratings with fixed spatial extent also embodies summation.

Although the model itself is agnostic to the form of summation, the fact that it captures both LF and RF data is not however inconsequential to the issue. We have already noted the many studies of RF detection that have come out in favour of a global mechanism. However, because we find that LF patterns, for which a global detection mechanism seems inherently unlikely, can be modelled similarly to RF patterns, we draw the more conservative conclusion that a dedicated global integration stage is also not involved in the detection of RF shapes.

The CFSF is key to accounting for the flattening of thresholds at intermediate and high frequencies. How does this compare to Poirier and Wilson's (2006) explanation of the flattening? Poirier & Wilson modelled their RF data using an intermediate stage comprising two broadly-tuned curvature sensitive mechanisms, one tuned to low, one to high RFs. The model threshold at each point along the frequency axis was that of the mechanism giving the lowest threshold, and this gave a good account of the flattening. Similarly, our CFSF may be considered as an umbrella describing the relative sensitivity to curvature of a number of curvature-sensitive mechanisms, the exact number of which we cannot specify. It is worth emphasising, however, that in our scheme the curvature-sensitive filters sensitive to the lowest frequencies are the ones with the highest sensitivity, and that the reason why the thresholds are so high at these points, especially for the RFs, is because of the relatively small values of physical curvature (per amplitude) in the stimuli.

The idea of a CFSF should not be deemed controversial. For every other dimension of our visual experience for which a modulation sensitivity function has been measured, whether luminance contrast, chromatic contrast, texture contrast, depth contrast, temporal contrast etc., sensitivity exhibits a high-frequency decline, the frequency at which the decline begins being dependent on the particular dimension in question as well as a range of spatial (e.g. eccentricity, age, light level etc.) and temporal (e.g. temporal frequency) factors. Doubtless too curvature. The half-cycle contours in our LF and RF patterns become increasingly shorter as modulation frequency increases, so it should not be surprising that the neural machinery that detects them also becomes increasingly less effective at representing them.

4.1. Limitations of model

Unlike some previous models of RF detection such as Poirier and Wilson's (2006) and Kempgens et al.'s (2013), which are filter-based models inspired by physiology, our model is based on the geometrical or mathematical properties of LF and RF pat-

terns. Mathematically, curvature is the rate of change of tangent orientation and is thus defined for an infinitesimal point on the waveform. Given that the human visual system contains finite-sized filter receptive fields, any model based on a mathematical definition of curvature is physiologically unrealistic. Nonetheless, the model presented here will hopefully serve as a basis for developing a more physiological model of LF and RF detection. There already exist candidate physiological models of curvature detectors. A number of studies have proposed that local curvature might be encoded by simple cell-like orientation selective filters arranged tangentially to form a curve (Gheorghiu & Kingdom, 2007, 2008, 2009; Poirier & Wilson, 2006; Hancock & Peirce, 2008; Kempgens et al., 2013; Zetzsche & Barth, 1990), with some models combining the outputs multiplicatively (or its mathematical equivalent) (Gheorghiu & Kingdom, 2009; Poirier & Wilson, 2006; Zetzsche & Barth, 1990). In both Poirier and Wilson's and Kempgens et al.'s models of RF detection, in which curvature is encoded by triplets of orientationally-selective filters, curvature is given additional sign-of-curvature selectivity by virtue of mutual antagonism between overlapping pairs of convex and concave triplets (though see Gheorghiu & Kingdom, 2008, for evidence to the contrary, at least for suprathreshold shapes). Such curvature-sensitive mechanisms could be the neural substrate for the extraction of curvature differences between points of curvature maxima and minimum in our model.

In some previous studies, the thresholds do not simply flatten but increase at the highest frequencies. Tyler's (1973) and Mullen et al.'s (2011) (in some cases) results show an upturn in thresholds for higher modulation frequencies: with Tyler (1973) at a frequency of about 3 c/deg for LF and with Mullen et al. (2011) in some cases a modulation frequency above 10 (cycles/360°) with both LF and RF. A similar slight increase in RF detection thresholds for higher modulation frequencies beyond 8 (cycles/360°) was also evident in some of Jeffrey et al.'s (2002) results. However, apart from the different stimulus characteristics, Jeffrey et al. (2002) only report data from three subjects, where just one of them shows a pronounced increase in thresholds. The increase in thresholds for high modulation frequencies is neither evident in Prins et al.'s (2007) LF results, nor in the data provided here, despite the fact that both Prins et al. and us measured thresholds for stimuli beyond 3 c/deg. In addition to the reported data, we conducted a control experiment to measure detection thresholds for RF and LF patterns with a modulation frequency of 30 for two additional naïve observers. Results show that thresholds are no higher than for a modulation frequency of 20. We suggest that the presence upturn observed in these previous studies at high frequencies may have been caused by display or stimulus limitations. Tyler (1973) generated his stimuli using an oscilloscope and the resolution limits of the apparatus might have caused the increase in thresholds at high frequencies. In the case of Mullen et al.'s (2011) study, the stimuli were defined by a fourth derivative luminance profile with a relatively low peak spatial frequency of 0.75 c/deg (2.4 deg radius), which resulted in stimuli with a much larger width than the narrow Gaussian profile ($\sigma = 0.05$ deg) employed here. It is reasonable to assume that the relatively wide contours used in Mullen et al.'s (2011) study led to an increase in detection thresholds for high frequency modulations because of a relatively low resolution limit for such stimuli. Of course, even with narrow contours there will eventually be a resolution limit. The CFSF model presented here does not predict the inevitable increase in thresholds at frequencies higher than those explored in the present study. To do so would require a CFSF with a somewhat different shape to the one shown in Fig. 4, one with an even more rapid decline at very high modulation frequencies. However, because we do not have the requisite data showing an upturn in thresholds at very high frequencies, we have not incorporated this feature into our present model of the CFSF.

In conclusion, our data and modeling suggest that the detection of shape modulations is processed by a common curvature-sensitive mechanism that is independent of whether the modulation is applied to a circle or a straight line.

Acknowledgments

We would like to thank the reviewers and Jonathan Victor for their many helpful comments, which led to numerous improvements of the manuscript. Results of this study were partly presented at the Vision Sciences Society Meeting (2016). This research was supported by a Natural Sciences and Engineering Research Council of Canada grant #RGPIN 121713-11 given to F.K.

References

Baldwin, A. S., Schmidtmann, G., Kingdom, F. A. A., & Hess, R. F. (2016). Rejecting probability summation for radial frequency patterns, not so Quick! *Vision Research, 122*, 124–134.

Bell, J., & Badcock, D. R. (2008). Luminance and contrast cues are integrated in global shape detection with contours. *Vision Research, 48*(21), 2336–2344. http://dx.doi.org/10.1016/j.visres.2008.07.015. http://doi.org/S0042-6989(08)00368-4 [pii].

Bell, J., Badcock, D., Wilson, H. R., & Wilkinson, F. (2007). Detection of shape in radial frequency contours: Independence of local and global form information. *Vision Research, 47*(11), 1518–1522.

Bell, J., Gheorghiu, E., Hess, R. F., & Kingdom, F. A. A. (2011). Global shape processing involves a hierarchy of integration stages. *Vision Research, 51*(15), 1760–1766.

Bell, J., Hancock, S., Kingdom, F. A. A., & Peirce, J. W. (2010). Global shape processing: Which parts form the whole? *Journal of Vision, 10*(6), 1–13.

Bell, J., Wilkinson, F., Wilson, H. R., Loffler, G., & Badcock, D. R. (2009). Radial frequency adaptation reveals interacting contour shape channels. *Vision Research, 49*(18), 2306–2317.

Brainard, D. H. (1997). The psychophysics toolbox. *Spatial Vision, 10*(4), 433–436.

Dickinson, J. E., Bell, J., & Badcock, D. R. (2013). Near their thresholds for detection, shapes are discriminated by the angular separation of their corners. *PLoS ONE, 8*(5), e66015.

Dickinson, J. E., McGinty, J., Webster, K. E., & Badcock, D. R. (2012). Further evidence that local cues to shape in RF patterns are integrated globally. *Journal of Vision, 12*(12), 16.

Dumoulin, S., & Hess, R. F. (2007). Cortical specialization for concentric shape processing. *Vision Research, 47*(12), 1608–1613.

Gheorghiu, E., & Kingdom, F. A. (2007). The spatial feature underlying the shape-frequency and shape-amplitude after-effects. *Vision Research, 47*, 834–844.

Gheorghiu, E., & Kingdom, F. A. (2008). Spatial properties of curvature-encoding mechanisms revealed through the shape-frequency and shape-amplitude after-effects. *Vision Research, 48*, 1107–1124.

Gheorghiu, E., & Kingdom, F. A. A. (2009). Multiplication in curvature processing. *Journal of Vision, 9*(2), 1–17. 23.

Green, D. M., & Swets, J. A. (1988). *Signal detection theory and psychophysics*. Los Altos, California: Peninsula Publishing.

Hancock, S., & Peirce, J. W. (2008). Selective mechanisms for simple contours revealed by compound adaptation. *Journal of Vision, 8*(7), 1–10. 11.

Hess, R. F., Achtman, R. L., & Wang, Y. (2001). Detection of constrast-defined shape. *Journal of the Optical Society of America A: Optics, Image Science, and Vision, 18*(9), 2220–2227.

Hess, R. F., Wang, Y., & Dakin, S. C. (1999). Are judgements of circularity local or global? *Vision Research, 39*(26), 4354–4360.

Jeffrey, B., Wang, Y., & Birch, E. (2002). Circular contour frequency in shape discrimination. *Vision Research, 42*(25), 2773–2779.

Kempgens, C., Loffler, G., & Orbach, H. S. (2013). Set-size effects for sampled shapes: Experiments and model. *Frontiers in Computational Neuroscience, 7*, 1–18.

Kingdom, F. A. A., Baldwin, A. S., & Schmidtmann, G. (2015). Modeling probability and additive summation for detection across multiple mechanisms under the assumptions of signal detection theory. *Journal of Vision, 15*(5), 1.

Kriegeskorte, N., Goebel, R., & Bandettini, P. (2006). Information-based functional brain mapping. *Proceedings of the National Academy of Sciences, 103*(10), 3863–3868.

Kriegeskorte, N., & Kievit, R. A. (2013). Representational geometry: Integrating cognition, computation, and the brain. *Trends in Cognitive Sciences, 17*(8), 401–412.

Kriegeskorte, N., Mur, M., & Bandettini, P. (2008). Representational similarity analysis – connecting the branches of systems neuroscience. *Frontiers in Systems Neuroscience, 2*(4), 1–28.

Laming, D. (2013). Probability summation – a critique. *Journal of the Optical Society of America A, 30*(3), 300–315.

Loffler, G., Wilson, H. R., & Wilkinson, F. (2003). Local and global contributions to shape discrimination. *Vision Research, 43*(5), 519–530.

Mullen, K. T., Beaudot, W. H. A., & Ivanov, I. V. (2011). Evidence that global processing does not limit thresholds for RF shape discrimination. *Journal of Vision, 11*(3), 1–21.
Nachmias, J. (1981). On the psychometric function for contrast detection. *Vision Research, 21*, 215–223.
Poirier, F. J. A. M., & Wilson, H. R. (2006). A biologically plausible model of human radial frequency perception. *Vision Research, 46*, 2443–2455.
Prins, N., & Kingdom, F.A.A., 2009. Palamedes: Matlab routines for analyzing psychophysical data. www.palamedestoolbox.org.
Prins, N., Kingdom, F. A. A., & Hayes, A. (2007). Detecting low shape-frequencies in smooth and jagged contours. *Vision Research, 47*(18), 2390–2402.
Quick, R. (1974). A vector-magnitude model of contrast detection. *Kybernetik, 16*(2), 65–67.
Salmela, V. R., Henriksson, L., & Vanni, S. (2016). Radial frequency analysis of contour shapes in the visual cortex. *PLOS Computational Biology, 12*(2), e1004719.
Schmidtmann, G., Kennedy, G. J., Orbach, H. S., & Loffler, G. (2012). Non-linear global pooling in the discrimination of circular and non-circular shapes. *Vision Research, 62*, 44–56.
Tan, K. W. S., Dickinson, J. E., & Badcock, D. R. (2013). Detecting shape change: Characterizing the interaction between texture-defined and contour-defined borders. *Journal of Vision, 13*(14), 1–16.
Tyler, C. W. (1973). Periodic vernier acuity. *The Journal of Physiology, 228*(3), 637–647.
Watson, A. B. (2013). A formula for the mean human optical modulation transfer function as a function of pupil size. *Journal of Vision, 13*(6), 18. 18.
Watt, R. J., & Andrews, D. P. (1982). Contour curvature analysis: Hyperacuities in the discrimination of detailed shape. *Vision Research, 22*, 449–460.
Wilkinson, F., James, T. W., Wilson, H. R., Gati, J. S., Menon, R. S., & Goodale, M. A. (2000). An fMRI study of the selective activation of human extrastriate form vision areas by radial and concentric gratings. *Current Biology: CB, 10*(22), 1455–1458. http://doi.org/S0960-9822(00)00800-9 [pii].
Wilkinson, F., Wilson, H. R., & Habak, C. (1998). Detection and recognition of radial frequency patterns. *Vision Research, 38*(22), 3555–3568.
Wilson, H. R. (1985). Discrimination of contour curvature: Data and theory. *Journal of the Optical Society of America A, 2*(7), 1191–1199.
Wilson, H. R., & Richards, W. A. (1989). Mechanisms of contour curvature discrimination. *Journal of the Optical Society of America A: Optics, Image Science, and Vision, 6*(1), 106–115.
Zetzsche, C., & Barth, E. (1990). Fundamental limits of linear filters in the visual processing of two-dimensional signals. *Vision Research, 30*, 1111–1117.